CrossMark

Detecting Interstellar Objects through Stellar Occultations

Amir Siraj and Abraham Loeb
Department of Astronomy, Harvard University, 60 Garden Street, Cambridge, MA 02138, USA; amir.siraj@cfa.harvard.edu, aloeb@cfa.harvard.edu

Abstract

Stellar occultations have been used to search for Kuiper Belt and Oort Cloud objects. We propose a search for interstellar objects based on the characteristic durations ($\sim$0.1 s) of their stellar occultation signals and high inclination relative to the ecliptic plane. An all-sky monitoring program of all $\sim$7 × 10^6 stars with $R \lesssim 12.5$ using 1-m telescopes with 0.1 s cadences is predicted to discover $\sim$1 interstellar object per year.

Unified Astronomy Thesaurus concepts: Minor planets (1065); Asteroids (72); Meteors (1041); Stellar occultation (2135)

1. Introduction

'Oumuamua was the first interstellar object (ISO) reported in the solar system (Meech et al. 2017; Micheli et al. 2018). Follow-up studies of 'Oumuamua were conducted to better understand its origin and composition (Bannister et al. 2017; Bolin et al. 2017; Gaidos et al. 2017; Jewitt et al. 2017; Mamajek 2017; Ye et al. 2017; Bialy & Loeb 2018; Fitzsimmons et al. 2018; Hoang et al. 2018; Trilling et al. 2018; Moro-Martín 2019; Sekanina 2019; Seligman et al. 2019; Siraj & Loeb 2019a, 2019b). 'Oumuamua's size was estimated to be $\lesssim$200 m, based on *Spitzer Space Telescope* constraints on its infrared emission given its expected surface temperature based on its orbit (Trilling et al. 2018).

In addition to 'Oumuamua, CNEOS 2014 January 8 (Siraj & Loeb 2019a) was tentatively the first interstellar meteor discovered that is larger than dust, and 2I/Borisov (Guzik et al. 2019) was the first confirmed interstellar comet.

Transient diffraction patterns caused by the occultation of a distant star due to an intervening small body have been proposed and used to search for Kuiper Belt objects (KBOs) and Oort Cloud objects (OCOs) in the solar system (Bailey 1976; Dyson 1992; Roques & Moncuquet 2000; Nihei et al. 2007; Schlichting 2009, 2012; Arimatsu 2019). Here, we propose an analogous search for ISOs, flagged by their unusual inclinations and unique kinematics leading a distribution of characteristic distribution of durations, the peak of which lies between that of KBOs and that of OCOs.

The data from such a search would calibrate population parameters for ISOs that are crucial for constraining formation theories of exoplanetary systems (Duncan et al. 1987; Charnoz & Morbidelli 2003; Veras et al. 2011, 2014; Pfalzner et al. 2015; Do et al. 2018; Raymond et al. 2018; Hands et al. 2019; Pfalzner & Bannister 2019; Siraj & Loeb 2019d). Below we derive the physical characteristics and rate of the expected ISO occultation events.

2. Theory

The measured intensity at wavelength λ from a diffraction pattern created by a spherical object of radius R_L at a distance D_L is

$$I_\rho(t) = \begin{cases} U_0^2(\rho, t/t_F) + U_1^2(\rho, t/t_F), & t/t_F \leqslant \rho, \\ 1 + U_1^2(\rho, t/t_F) + U_2^2(\rho, t/t_F) \\ -2U_1(\rho, t/t_F)\sin\dfrac{\pi}{2}(\rho^2 + (t/t_F)^2) \\ +2U_2(\rho, t/t_F)\cos\dfrac{\pi}{2}(\rho^2 + (t/t_F)^2), & t/t_F \geqslant \rho, \end{cases}$$
(1)

where $\rho = (R_L/F)$ is the radius of the object in units of the Fresnel scale $F = \sqrt{\lambda D_L/2}$, and t_F is the Fresnel scale crossing time for the object (Roques et al. 1987; Nihei et al. 2007). For a transverse speed, $v_\perp$, at a distance D_L, the Fresnel time is $t_F = 0.12$ s $(D_L/20\,\mathrm{au})^{1/2}$ $(v_\perp/10\,\mathrm{km\,s}^{-1})^{-1}$ $(\lambda/\mu\mathrm{m})^{1/2}$ and the Fresnel scale is $F = 1.2$ km $(D_L/20\,\mathrm{au})^{1/2}$ $(\lambda/\mu\mathrm{m})^{1/2}$. The Lommel functions are defined as

$$U_n(\mu, \nu) = \sum_{k=0}^{\infty} (-1)^k \left(\frac{\mu}{\nu}\right)^{n+2k} J_{n+2k}(\pi\mu\nu),$$
(2)

where J_n is a Bessel function of order n. With regard to the impact parameter b, we assume $b = 0$ for simplicity. Figure 1 shows lightcurves for different values of ρ, as well as lightcurves sampled as at a spatial resolution of F. While the calculated lightcurves represent monochromatic light, the finite filters used in practice slightly reduces the statistical power.

For a solar-type star with an R magnitude of 12, the flux of R-band photons at Earth is $\sim$2.8 × 10^5 m^{-2} s^{-1}. For an intensity dip caused by an occultation event, a signal-to-noise ratio of $\gtrsim$10 for a telescope with 1 m^2 collecting area with a temporal resolution of t_f would require the intensity dip to be $\gtrsim$6%, corresponding to $\rho \gtrsim 0.22$. The appropriate values of $\rho_{\min}$ as a function of magnitude are listed in Table 1.

In addition to $\rho \geqslant \rho_{\min}$ for a strong signal, we also require the occulting object to subtend a larger angular size on the sky than the star to avoid dilution of the signal by the finite source size. We adopt the conservative condition $R_L \leqslant 10$ km for ISOs. Given a star of radius R_S and distance D_L, the three conditions for an ISO occultation event are expressed as follows:
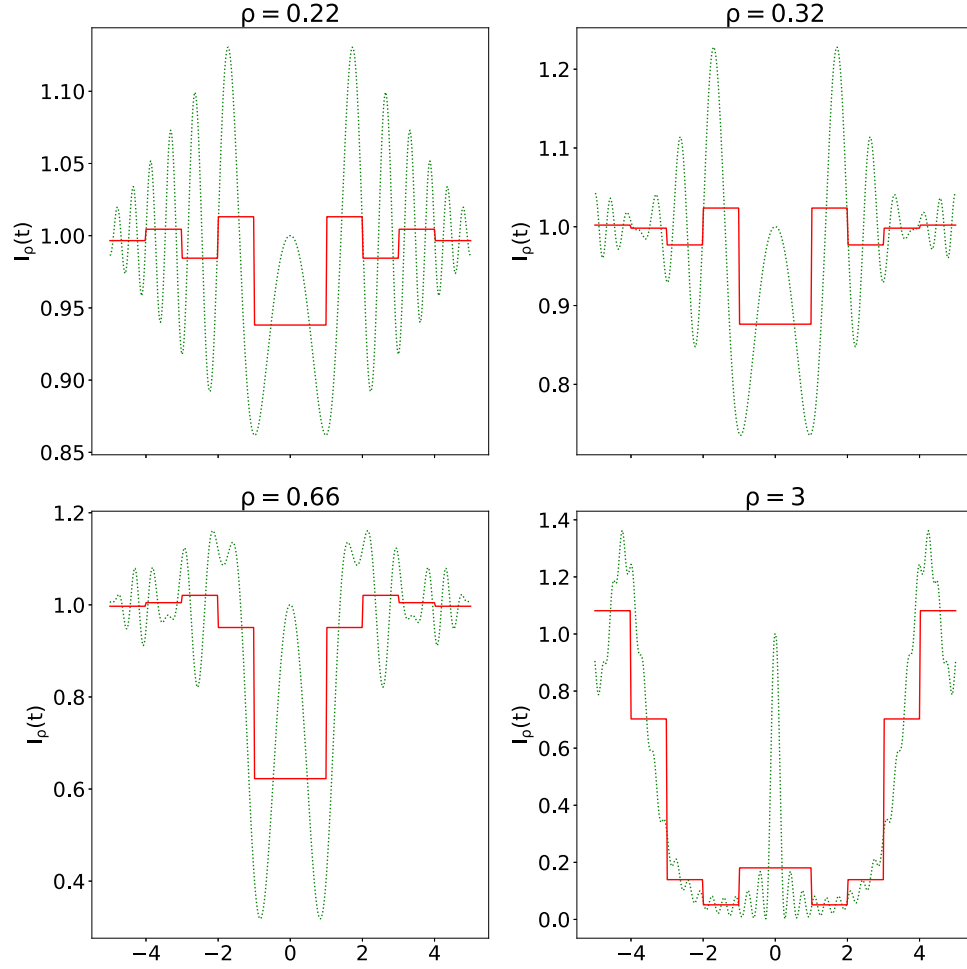
$$R_L > \rho_{\min} \sqrt{\frac{\lambda D_L}{2}},$$
(3)

Figure 1. Occultation lightcurves for the values of $\rho_{\min}$ (ratio of ISO radius to the Fresnel scale) in Table 1 (dotted green lines), and sampled lightcurves at temporal resolution, t_F (solid red lines). For a transverse speed $v_\perp$ at a distance D_L, the time unit, $t_F = 0.1$ s $(D_L/20$ au$)^{1/2}$ $(v_\perp/10$ km s$^{-1})^{-1}$.

Table 1
Background Photon Flux, Maximum Dip in Intensity, and Minimum Value of ρ for Occultation Events with Solar-type Background Stars, Assuming a 1 m^2 Collecting Area and a Temporal Resolution of t_f

R Magnitude	R-band Photon Flux (m^{-2} s^{-1})	$\Delta I_{\min}$ (%)	$\rho_{\min}$
12	2.8×10^5	6	0.22
14	4.4×10^4	15	0.32
16	6.9×10^3	38	0.66
18	1.1×10^3	95	3

$$\frac{R_L}{D_L} > \frac{R_S}{D_S}, \tag{4}$$

$$R_L < 10 \text{ km.} \tag{5}$$

Figure 2 illustrates a parameter space in which all three conditions are satisfied.

We approximate the cumulative number density of ISOs as a power law with exponent -3.3, calibrated by the number density ($n_O \sim 0.2$ au^{-3}) of 'Oumuamua size ($R_O \sim 100$ m) objects (Landgraf et al. 2000; Do et al. 2018; Siraj & Loeb 2019c).

We adopt the three-dimensional velocity dispersion of stars in the thin disk of the Milky Way as a proxy for the kinematics of ISOs, each corresponding to the standard deviation of a Gaussian distribution about the local standard of rest:
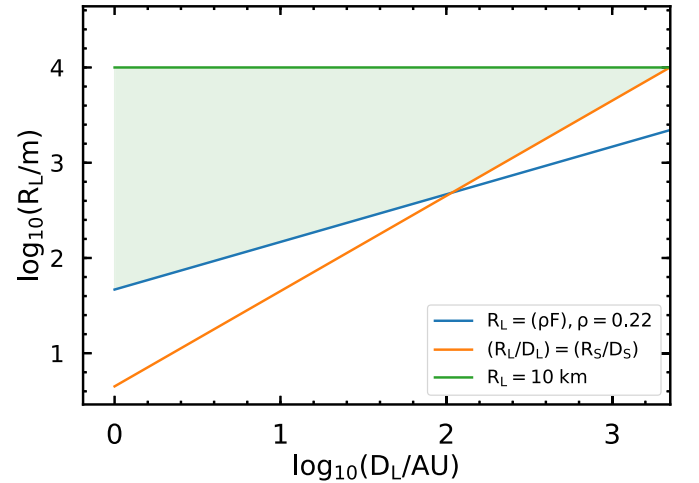

Figure 2. Parameter space in which conditions (3), (4), and (5), are satisfied for a $R = 12$ solar-type star. $R_S \sim R_\odot$ and $D_S \sim 300$ pc for an $R = 12$ solar-type star.

$\sigma_x = 35$ km s^{-1}, $\sigma_y = 25$ km s^{-1}, $\sigma_z = 25$ km s^{-1} (Bland-Hawthorn & Gerhard 2016). The resulting distribution of observed transit speeds (once the motion of the Earth is subtracted) has a mean value of $\bar{v}_{\text{obs}} \sim 40$ km s^{-1}.
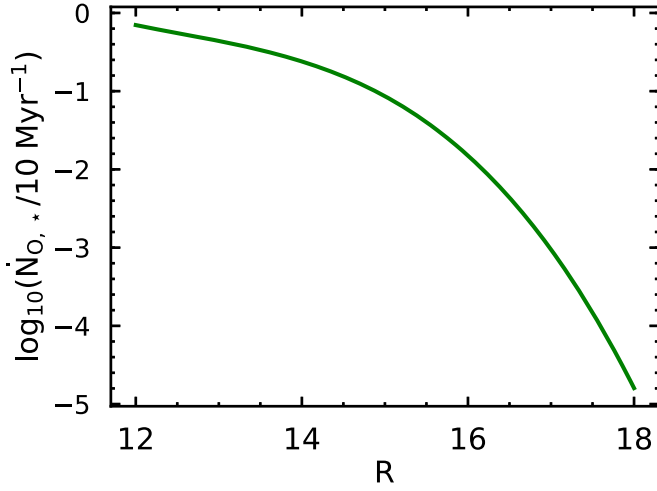
Figure 3. ISO occultation rate per star as a function of R magnitude for solar-type stars.

Figure 4. ISO occultation rate per star as a function of stellar radius, for a $R = 12$ star.

The rate of occultations per star is given by

$$\dot{N}_{O,\star} \approx 2\pi \int_{1\,\text{au}}^{L_1} n_O \left[\left(\frac{\rho_{\min} \sqrt{\lambda D_L/2}}{R_O} \right)^{-3.3} - \left(\frac{R_{\max}}{R_O} \right)^{-3.3} \right]$$
$$\times \left(\frac{\bar{v}_{\text{obs}} D_L R_S}{D_S} \right) dD_L$$
$$+ 2\pi \int_{L_1}^{L_2} n_O \left[\left(\frac{R_S D_L}{D_S R_O} \right)^{-3.3} - \left(\frac{R_{\max}}{R_O} \right)^{-3.3} \right]$$
$$\times \left(\frac{\bar{v}_{\text{obs}} D_L R_S}{D_S} \right) dD_L,$$

(6)

where the limits of the integrals, L_1 and L_2, are defined as follows:

$$L_1 = \begin{cases} \frac{\rho_{\min}^2 \lambda D_S^2}{2R_S^2}, & \frac{\rho_{\min}^2 \lambda D_S^2}{2R_S^2} \leqslant \frac{R_{\max} D_S}{R_S}, \\ \frac{2R_{\max}^2}{\rho_{\min}^2 \lambda}, & \frac{\rho_{\min}^2 \lambda D_S^2}{2R_S^2} \geqslant \frac{R_{\max} D_S}{R_S}, \end{cases}$$

(7)

$$L_2 = \begin{cases} \frac{R_{\max} D_S}{R_S}, & \frac{\rho_{\min}^2 \lambda D_S^2}{2R_S^2} \leqslant \frac{R_{\max} D_S}{R_S}, \\ 0, & \frac{\rho_{\min}^2 \lambda D_S^2}{2R_S^2} \geqslant \frac{R_{\max} D_S}{R_S}. \end{cases}$$

(8)

The resulting ISO occultation rate per star as a function of magnitude is shown in Figure 3, and corresponds to $\sim 0.1\,\text{Myr}^{-1}$ at $R = 12$. For an $R = 12$ star, Figure 4 shows the ISO occultation rate as a function of stellar radius.

To determine how easily discernible ISO, KBO, and OCO occultation signatures are from each other, and to understand the distribution of timescales on which ISO occultations occur, we numerically simulated the distribution of expected Fresnel distance crossing times for each population, assuming a $R = 12$ solar-type star.

We draw distances from the distribution $P(D_L) \propto D_L^2$ with bounds of 1 au to $(R_{\max} D_S/R_S)$ for ISOs, bounds of 30–50 au for KBOs, and bounds of 2×10^3 to 10^5 au for OCOs. We draw velocities from the aforementioned kinematics for ISOs; we compute the orbital speed corresponding the distance for
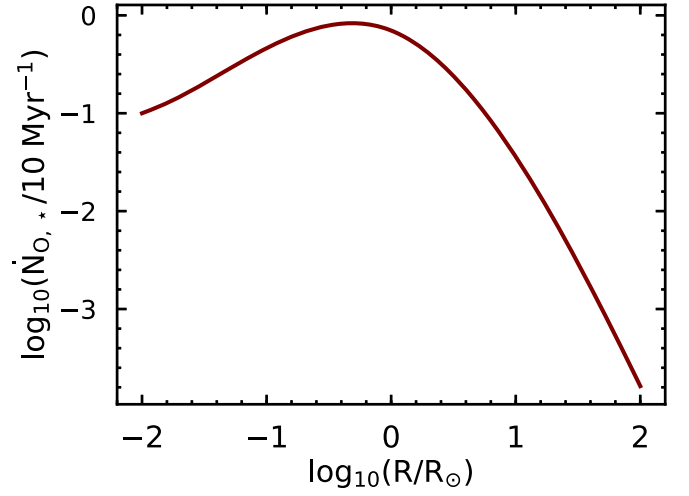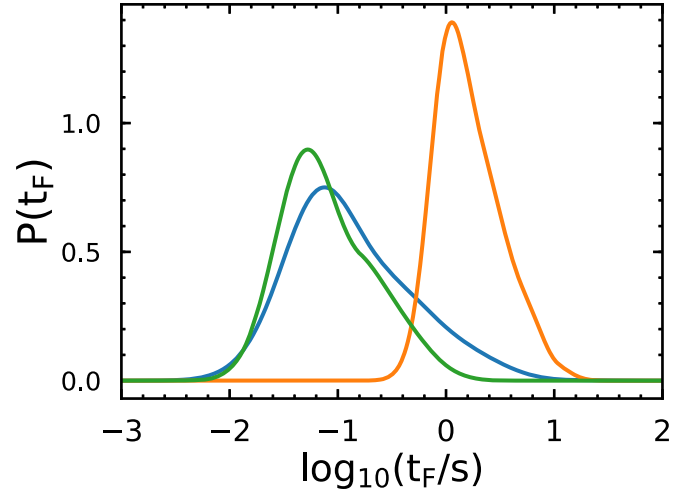

Figure 5. Expected probability distribution of Fresnel crossing times during stellar occultations observed from Earth for ISOs (blue), KBOs (green), and OCOs (orange), for a $R = 12$ solar-type star.

KBOs and for OCOs. We do not consider gravitational focusing and acceleration by the Sun for ISOs, as these effects would only be significant at $D_L \lesssim 1$ au. We sample random points in the Earth's orbit to obtain the motion of the observer relative to the object. We draw sizes for each population from a power-law distribution with index ~ -3, with the appropriate bounds for each population. If conditions (4) and (5) are satisfied, we compute the Fresnel distance crossing time, $t_F = (F/v_\perp)$. Otherwise, we re-draw distance and size. The resulting distributions of t_F are shown in Figure 5. ISO occultation events have have an even distribution with distance between 1 and $\sim 10^3$ au. We find that the timescales for ISO and OCO occultation events are distinct. The ISO timescale distribution peaks at $t_F = 0.1$ s, and a survey can avoid KBOs by pointing away from the plane of the ecliptic.

3. Conclusions

There are $\sim 7 \times 10^6$ stars in a with magnitude $R \lesssim 12.5$ (McMillan 2018). An all-sky network of 1 m telescopes continuously monitoring all $R = 12$ stars with a time resolutions of 0.1 s should yield a discovery rate of ~ 1 ISO

3

per year. This would be a significant improvement on the current discovery rate of an ISO every few years. Our method supplements direct detection through reflected sunlight but nearby events could benefit from both methods of detection. By measuring each occultation in two or three colors, the radius and distance of the occulting object can be constrained (Dyson 1992).

The data from such a survey would provide invaluable new information on the size distribution, composition, and possible origin of ISOs. Such information would be particularly valuable given the puzzle of the first two confirmed ISOs, 'Oumuamua and Borisov, having such different physical characteristics (Meech et al. 2017; Guzik et al. 2019), and given the high implied abundance of ISOs relative to previous predictions (Moro-Martin et al. 2009).

ORCID iDs

Amir Siraj ⬤ https://orcid.org/0000-0002-9321-6016
Abraham Loeb ⬤ https://orcid.org/0000-0003-4330-287X

References

Arimatsu, K. 2019, NatAs, 3, 301
Bailey, M. 1976, Natur, 259, 290
Bannister, M. T., Schwamb, M. E., Wesley, C. F., et al. 2017, ApJL, 851, L38
Bialy, S., & Loeb, A. 2018, ApJL, 868, L1
Bland-Hawthorn, J., & Gerhard, O. 2016, ARA&A, 54, 529
Bolin, B. T., Weaver, H. A., Fernandez, Y. R., et al. 2017, ApJL, 852, L2
Charnoz, S., & Morbidelli, A. 2003, Icar, 166, 141
Do, A., Tucker, M. A., & Tonry, J. 2018, ApJL, 855, L10
Duncan, M., Quinn, T., & Tremaine, S. 1987, AJ, 94, 1330
Dyson, M. 1992, QJRAS, 33, 45
Engelhardt, T., Jedicke, R., Vereš, P., et al. 2017, AJ, 153, 133
Fitzsimmons, A., Snodgrass, C., Rozitis, B., et al. 2018, NatAs, 2, 133
Gaidos, E., Williams, J., & Kraus, A. 2017, RNAAS, 1, 13
Guzik, P., Drahus, M., Rusek, K., et al. 2020, NatAs, 4, 53
Hands, T. O., Dehnen, W., Gration, A., Stedel, J., & Moore, B. 2019, MNRAS, 490, 21
Hoang, T., Loeb, A., Lazarian, A., & Cho, J. 2018, ApJ, 860, 42
Jewitt, D., Luu, J., Rajagopal, J., et al. 2017, ApJL, 850, L36
Landgraf, M., Baggaley, W. J., Grun, E., Kruger, H., & Linkert, G. 2000, JGR, 105, 10343
Mamajek, E. 2017, RNAAS, 1, 21
McMillan, P. J. 2018, RNAAS, 2, 51
Meech, K. J., Weryk, R., Micheli, M., et al. 2017, Natur, 552, 378
Micheli, M., Farnocchia, D., Meech, K. J., et al. 2018, Natur, 559, 223
Moro-Martin, A. 2019, ApJ, 157, 86
Moro-Martin, A., Turner, E. L., & Loeb, A. 2009, ApJ, 704, 733
Nihei, M., Lehner, M. J., Bianco, F. B., et al. 2007, AJ, 134, 1596
Pfalzner, S., & Bannister, M. T. 2019, ApJL, 874, L34
Pfalzner, S., Parmentier, G., Steinhausen, M., Vincke, K., & Menten, K. 2015, ApJ, 794, 147
Raymond, S. N., Armitage, P. J., Veras, D., Quintana, E. V., & Barclay, T. 2018, MNRAS, 476, 3031
Roques, F., & Moncuquet, M. 2000, Icar, 147, 530
Roques, F., Moncuquet, M., & Sicardy, B. 1987, AJ, 93, 1549
Schlichting, H. E. 2009, Natur, 462, 895
Schlichting, H. E. 2012, ApJ, 761, 150
Sekanina, Z. 2019, arXiv:1901.08704
Seligman, D., Laughlin, G., & Batygin, K. 2019, ApJL, 876, L26
Siraj, A., & Loeb, A. 2019a, ApJL, 872, L10
Siraj, A., & Loeb, A. 2019b, RNAAS, 3, 15
Siraj, A., & Loeb, A. 2019c, arXiv:1904.07224
Siraj, A., & Loeb, A. 2019d, arXiv:1906.03270
Trilling, D., Mommert, M., Hora, J. L., et al. 2018, AJ, 156, 261
Veras, D., Evans, N. W., Wyatt, M. C., & Tout, C. A. 2014, MNRAS, 437, 1127
Veras, D., Wyatt, M. C., Mustill, A. J., Bonsor, A., & Eldridge, J. J. 2011, MNRAS, 417, 2104
Ye, Q.-Z., Zhang, Q., Kelley, M. S. P., & Brown, P. G. 2017, ApJL, 851, L5